Ultrasonic Attenuation in Oblique Magnetic Fields*†

MICHAEL P. GREENE, ALLAN R. HOFFMAN‡, A. HOUGHTON, AND J. J. QUINN
Physics Department, Brown University, Providence, Rhode Island
(Received 28 November 1966)

The propagation of acoustic waves at oblique angles to a dc magnetic field in a material with an arbitrary closed Fermi surface is studied. In addition to the conventional geometric resonances, absorption edges due to Doppler-shifted cyclotron resonance, and geometric resonances associated with nonextremal orbits on the Fermi surface can occur. A formal theory is developed and applied to two simple models of the ground state of potassium: the free-electron model and the spin-density-wave model. Experimental results on the attenuation of 60-Mc/sec longitudinal acoustic waves in potassium are presented and compared with the predictions of both models. The experimental results appear to favor the free-electron model, but they are not definitive in view of the low value of ql, the product of acoustic wave number and electron mean free path, attained in the experiments. The general features of the attenuation as a function of magnetic field for a fixed oblique angle, which agree well with the detailed theory, are discussed in terms of a simple intuitive picture.

I. INTRODUCTION

MOST experimental and theoretical studies of the magnetic field dependence of ultrasonic attenuation in metals have been restricted to propagation either perpendicular or parallel to the magnetic field. Notable exceptions are the theoretical work of S. Eckstein[1] and Kaner,[2] and Y. Eckstein's[3] experimental studies of acoustic attenuation at oblique angles to the magnetic field in antimony and arsenic. For oblique propagation, absorption edges due to Doppler-shifted cyclotron resonance, as well as geometric resonances in the acoustic attenuation, can occur. Doppler-shifted cyclotron resonance is possible when the condition

$$n\omega_c < |\mathbf{q}\cdot\mathbf{v}_M| \pm \omega \tag{1}$$

is satisfied for $n=1, 2, \cdots$. Here ω and ω_c are the acoustic and electron cyclotron frequencies, respectively; $\mathbf{q}$ is the wave vector of the sound wave, and $\mathbf{v}_M$ the maximum electron velocity parallel to the dc magnetic field. Absorption edges in the attenuation as a function of dc magnetic field strength occur because, for any given value of the integer n, there is a maximum field B_n, above which the inequality (1) is no longer satisfied. Thus, as the magnetic field is decreased through a value of B_n, the acoustic attenuation should increase. Both the increase in attenuation due to an absorption edge and the amplitude of the magnetoacoustic oscillations depend upon the angle between $\mathbf{q}$ and $\mathbf{B}$, being zero for parallel propagation and increasing with increasing angle. The values of the magnetic field at the absorption edges and at the maxima and minima of the magnetoacoustic oscillations also depend on the angle between $\mathbf{q}$ and $\mathbf{B}$.

In Fig. 1 we give a plot, as a function of θ, of the expected values of ω_c/qv_F associated with the first few absorption edges, and with the first few maxima and minima of the magnetoacoustic oscillations. These curves are based on the free-electron model where v_F is the Fermi velocity. The heavy lines are the $n=1$ and $n=2$ Doppler-shifted cyclotron resonance absorption edges. The light lines depict the positions of the maxima and minima associated with the conventional geometric resonances, which are usually studied at perpendicular

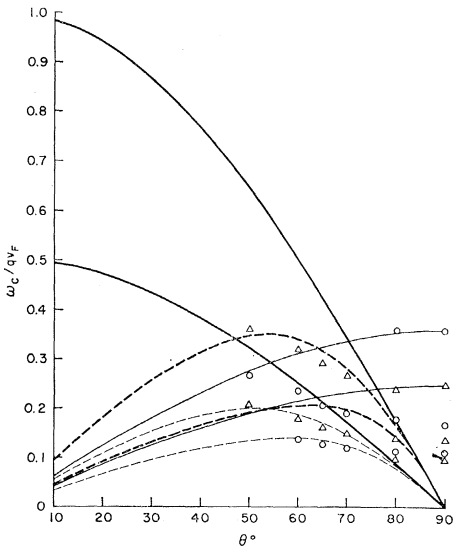

FIG. 1. A plot of the values of the parameter ω_c/qv_F associated with various "resonances" as a function of θ, the angle between $\mathbf{q}$ and $\mathbf{B}$. The curves are based on the intuitive picture described in Sec. V of the text. The heavy lines are the $n=1$ and $n=2$ Doppler-shifted cyclotron resonance absorption edges; for both, ω_c/qv_F varies as $\cos\theta$. The light lines are the extrema associated with the conventional ($n=0$) geometric resonances; these curves vary as $\sin\theta$. The heavy and light dashed lines are the geometric resonances associated with the $n=1$ and $n=2$ Doppler-shifted cyclotron absorption. The triangles and circles indicate the positions of the experimentally observed maxima and minima, respectively.

* Supported in part by the Advanced Research Projects Agency, the Air Force Office of Scientific Research and the U. S. Army Research Office, Durham, North Carolina.

† The research reported in this article is based in part on a thesis submitted by A. R. Hoffman in partial fulfillment of the requirements for the degree of Doctor of Philosophy at Brown University.

‡ National Aeronautics and Space Administration Trainee.

[1] S. G. Eckstein, Phys. Rev. Letters **12**, 360 (1964); Phys. Letters **20**, 142 (1966).

[2] E. A. Kaner, Zh. Eksperim. i Teor. Fiz. **43**, 216 (1962) [English transl.: Soviet Phys.—JETP **16**, 154 (1963)].

[3] Y. Eckstein, Phys. Letters **20**, 144 (1966).

propagation. The heavy and light dashed lines indicate the locations of magneto-acoustic extrema associated with the $n=1$ and $n=2$ Doppler-shifted cyclotron resonances. A detailed discussion of this figure is deferred until the discussion of the experimental results. At this point it is sufficient to remark that at reasonably large angles ($\theta>50°$), where the increase in attenuation associated with the absorption edge is large, the edge itself lies within or near the region of the magneto-acoustic resonances. Because of this, and because of the broadening of the edge resulting from the finite electron collision time, it becomes impossible, even for the free-electron model, to locate the position of the edge without a detailed calculation. Such a calculation and its comparison with experiment and with the intuitive picture of Fig. 1 is one of the objectives of the present work.

In order to explain some rather perplexing data[4] on the optical reflectivity of potassium, Overhauser[5] has suggested that the alkali metals might be examples of the spin-density-wave (SDW) state. To obtain agreement with the de Haas–van Alphen studies of Shoenberg and Stiles,[6] Overhauser has predicted that the axis of the SDW will line up parallel to a sufficiently strong magnetic field. This leaves the extremal cross-sectional area of the Fermi surface, which is measured by the de Haas–van Alphen effect, essentially unchanged, but it dramatically affects the Fermi surface near the spin-density-wave energy gap. In Fig. 2 we plot v_z, the electron velocity parallel to the dc magnetic field, as a function of k_z for both the free-electron model and SDW model. It can easily be seen that the maximum velocity, v_M, is smaller in the SDW model than in the free-electron model. The difference amounts to about 18% in potassium. From the inequality (1), it is apparent that the position of an absorption edge gives a measure of v_M, the maximum electron velocity in the direction of **B**.

It should be noted that the spin-density-wave model of potassium is by no means universally accepted; in fact, recent theoretical work by Hamann and Overhauser,[7] Penn and Cohen,[8] and Fedders and Martin,[9] have raised questions concerning the existence of such a state in simple metals. Therefore an experimental test of the spin-density-wave hypothesis is desirable. For this reason, we have carried out detailed numerical calculations of the attenuation for both a free-electron model and a SDW model appropriate to potassium. Comparison of these with experimental data should serve to test the validity of Overhauser's spin-density-wave hypothesis for potassium. In addition, it provides an opportunity to study quantitatively the effect of a nonspherical Fermi surface on the attenuation.

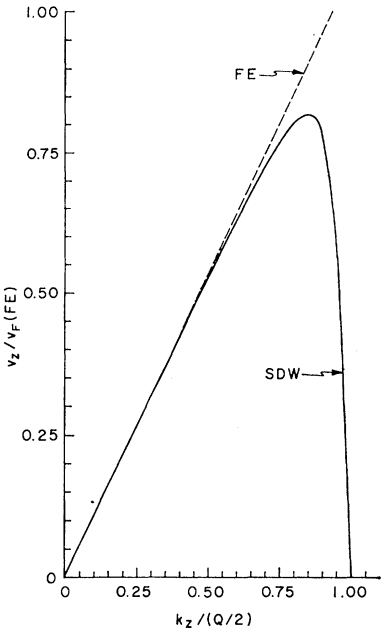

FIG. 2. A graph of v_z, the velocity parallel to the magnetic field, versus wave number k_z. The ordinate is measured in units of the free-electron Fermi velocity, the abscissa in units of $\frac{1}{2}Q$, where Q is the SDW wave vector. The solid line is the prediction of the SDW model, the dashed line that of the free-electron model.

The comparison of our experimental results with an SDW model of potassium requires some generalization of standard treatments of acoustic attenuation for a free-electron gas.[10] In the second section of this paper, we outline the general semiclassical theory of acoustic attenuation for an arbitrary closed Fermi surface in the presence of an oblique magnetic field. In the third section, the general theory is applied to both a SDW model and a free-electron model appropriate to potassium. Numerical results, for both models, of the attenuation as a function of magnetic field for various angles of propagation are presented. The fourth section describes briefly the experimental technique and experimental conditions. The fifth section is a comparison of the experimental data with the results of both the free electron and SDW models. A discussion is presented of how the important parameter ql, the product of acoustic wave vector and electron mean free path, is determined for each model. An interpretation of the experimental results in terms of the simple picture of Fig. 1 is given. The final section is a summary of our results and discussion of the conclusions that can be drawn from them.

II. ATTENUATION COEFFICIENT FOR AN ARBITRARY FERMI SURFACE

In order to compute the acoustic attenuation coefficient for potassium in a SDW state, it is necessary to develop a formalism capable of treating ultrasonic propagation at arbitrary angles to a dc magnetic field **B** for materials with a nonspherical Fermi surface. In

[4] H. Mayer and M. H. El Naby, Z. Physik **174**, 280 (1963); **174**, 289 (1963); M. H. El Naby, *ibid.* **174**, 269 (1963).
[5] A. W. Overhauser, Phys. Rev. Letters **13**, 190 (1964); Phys. Rev. **128**, 1437 (1962).
[6] D. Shoenberg and P. Stiles, Proc. Roy. Soc. (London) **A281**, 62 (1964).
[7] D. R. Hamann and A. W. Overhauser, Phys. Rev. **143**, 183 (1966).
[8] D. R. Penn and M. H. Cohen (to be published).
[9] P. A. Fedders and P. C. Martin, Phys. Rev. **143**, 245 (1966).
[10] M. H. Cohen, M. J. Harrison, and W. A. Harrison, Phys. Rev. **117**, 936 (1960).

this section we develop the general theory and apply it to the specific cases of SDW and free-electron models.

Blount[11] has shown that the average power removed from the ultrasonic wave is equal, in the steady state, to Q, the net power delivered to the lattice by electrons per cycle of the sound wave. As is well known, the attenuation coefficient is given by

$$\alpha = Q/(\tfrac{1}{2}NM|u|^2 v_s), \tag{2}$$

where N is the density of ions of mass M, v_s is the sound velocity, and $\mathbf{u}$ is the velocity of the ions. In general Q can be written in the form

$$Q = \tfrac{1}{2}\,\mathrm{Re}\{\mathbf{j}_e^* \cdot \mathcal{E} - \mathbf{u}^* \cdot \langle \mathbf{p}(\partial f/\partial t)_{\mathrm{coll}}\rangle_{\mathrm{cy}}\}. \tag{3}$$

In this equation the first term is the Joule heat produced by the electronic current $\mathbf{j}_e$ in the presence of the self-consistent field $\mathcal{E}$. The second term is the power returned to the electrons by the moving lattice; the quantity $\langle \mathbf{p}(\partial f/\partial t)_{\mathrm{coll}}\rangle_{\mathrm{cy}}$ is the average over one cycle of the sound wave of the product of the electronic momentum and the rate of change of the electron distribution function, f, due to collisions. We express Maxwell's equations in the form[12]

$$\mathbf{J} = -\boldsymbol{\Gamma} \cdot \mathcal{E}, \tag{4}$$

where

$$\boldsymbol{\Gamma} = \frac{ic^2q^2}{4\pi\omega}\left(\frac{\omega^2}{c^2q^2} - 1\right)\mathbf{1} + \frac{ic^2}{4\pi\omega}\mathbf{qq} \tag{5}$$

and $\mathbf{J}$, the total current in the system, is given by

$$\mathbf{J} = \mathbf{j}_e + Ne\mathbf{u}. \tag{6}$$

Using Eqs. (5) and (6) we can write the power Q as

$$Q = -\tfrac{1}{2}\,\mathrm{Re}\{Ne\mathbf{u}^* \cdot [\mathcal{E} + (1/Ne)\langle \mathbf{p}(\partial f/\partial t)_{\mathrm{coll}}\rangle_{\mathrm{cy}}]\}. \tag{7}$$

In order to proceed further, it is necessary to determine the electronic distribution function f. To do this for an arbitrary Fermi surface, we integrate the Boltzmann equation following a prescription given by Eckstein.[13] The Boltzmann equation is written

$$\frac{\partial f}{\partial t} + \mathbf{v} \cdot \boldsymbol{\nabla} f - \frac{e}{\hbar}\left(\mathcal{E} + \frac{1}{c}\mathbf{v} \times \mathbf{B}\right) \cdot \boldsymbol{\nabla}_{\mathbf{k}} f = \left(\frac{\partial f}{\partial t}\right)_{\mathrm{coll}}. \tag{8}$$

It will be assumed that the principal scattering mechanism is the elastic collisions of the electrons with impurities fixed in the moving lattice. These collisions tend to relax the distribution function to a local equilibrium value $\bar{f}_0 = f_0(E',\zeta')$, where f_0 is the Fermi function, $\zeta'(\mathbf{r},t)$ is the local chemical potential and E' is the energy measured in the center-of-mass system of the impurities. This coordinate system is displaced in $\mathbf{k}$ space relative to the laboratory system by an amount $\hbar^{-1}m\mathbf{u}$. Under these conditions, the collision term in Eq. (8) can be approximated by

$$(\partial f/\partial t)_{\mathrm{coll}} = -(f - \bar{f}_0)/\tau, \tag{9}$$

where $\tau = \tau(E',k')$ serves as a relaxation time. We now define f_2 as the deviation of the local equilibrium distribution function from the value $f_0(E,\zeta_0)$, the thermal equilibrium value in the absence of the sound wave,

$$f_2 = \bar{f}_0 - f_0(E,\zeta_0). \tag{10}$$

In this equation, E and ζ_0 are the electronic energy and chemical potential in the absence of the sound wave. By expanding all quantities to first order in the amplitude of the sound wave, we obtain

$$f_2 = -(\partial f_0/\partial E)[m\mathbf{v} \cdot \mathbf{u} + \zeta_1], \tag{11}$$

where $\mathbf{v} = (1/\hbar)(\partial E/\partial \mathbf{k})$ is the electron velocity, and $\zeta_1 = \zeta' - \zeta_0$. As we shall see, the first term in the brackets of Eq. (11) contributes to the conventional collision drag effect, and the second term to the diffusion current. If we now write $f = f_0(E,\zeta_0) + f_1$, and further assume that all quantities of first order in the amplitude of the sound wave vary in space and time as $\exp(i\mathbf{q} \cdot \mathbf{r} - i\omega t)$, the Boltzmann equation becomes

$$i\omega f_1 - i\mathbf{q} \cdot \mathbf{v} f_1 - e\mathbf{v} \cdot \mathcal{E}\frac{\partial f_0}{\partial E} - \frac{e}{\hbar c}(\mathbf{v} \times \mathbf{B}) \cdot \boldsymbol{\nabla}_{\mathbf{k}} f_1 + \frac{f_1 - f_2}{\tau} = 0. \tag{12}$$

Following Eckstein,[13] it is convenient to introduce a parameter s, with the dimensions of time, which describes the position of an electron on its orbit perpendicular to $\mathbf{B}$. It can be shown that

$$\frac{\partial f_1}{\partial s} = -\frac{e}{\hbar c}\mathbf{v} \times \mathbf{B} \cdot \boldsymbol{\nabla}_{\mathbf{k}} f_1, \tag{13}$$

and therefore Eq. (12) becomes

$$\frac{\partial f_1}{\partial s} + i\left(\omega - \mathbf{q} \cdot \mathbf{v} - \frac{i}{\tau}\right) f_1 = \left(e\mathcal{E} \cdot \mathbf{v} - \frac{m\mathbf{v} \cdot \mathbf{u}}{\tau} - \frac{\zeta_1}{\tau}\right)\frac{\partial f_0}{\partial E}. \tag{14}$$

This equation may now be solved by using the integrating factor

$$\exp\left\{\int_0^s \left[\frac{1}{\tau} + i\omega - i\mathbf{q} \cdot \mathbf{v}(l)\right] dl\right\}$$

to give

$$f_1(E,k_z,s) = \int_{-\infty}^{s} ds' \left[e\mathcal{E} \cdot \mathbf{v}(s') - \frac{m\mathbf{v}(s') \cdot \mathbf{u}}{\tau} - \frac{\zeta_1}{\tau}\right]\frac{\partial f_0}{\partial E} \times \exp\left[\left(\frac{1}{\tau} + i\omega\right)(s' - s) + i\mathbf{q} \cdot (\mathbf{R} - \mathbf{R}')\right], \tag{15}$$

[11] E. I. Blount, Phys. Rev. **114**, 418 (1959).

[12] We assume a time and space dependence of the form $\exp(i\mathbf{q} \cdot \mathbf{r} - \omega t)$.

[13] S. G. Eckstein, Bull. Am. Phys. Soc. **9**, 550 (1964).

and the electronic current density

$$j_e=\frac{2}{(2\pi)^3}\int d^3k(-e\mathbf{v}f_1)$$
$$=\frac{-e^2B}{4\pi^3\hbar^2c}\int_0^\infty dE\int_{-\infty}^\infty dk_z\int_0^{2\pi/\omega_c} ds\,\mathbf{v}(s)\int_{-\infty}^s ds'$$
$$\times\left[e\mathcal{E}\cdot\mathbf{v}(s')-\frac{m\mathbf{v}(s')\cdot\mathbf{u}}{\tau}-\frac{\zeta_1}{\tau}\right]\left(\frac{\partial f_0}{dE}\right)$$
$$\times\exp\left[\left(\frac{1}{\tau}+i\omega\right)(s'-s)+i\mathbf{q}\cdot(\mathbf{R}-\mathbf{R}')\right]. \quad (16)$$

In these equations $\omega_c=eB/m^*(E,k_z)c$, where m^* is the cyclotron effective mass. It has also been assumed that $\mathbf{B}$ is in the z direction.

We continue by separating the position vector $\mathbf{R}$ and velocity $\mathbf{v}$ into their periodic and aperiodic parts, $\mathbf{R}=\mathbf{R}_p+\mathbf{R}_a=\mathbf{R}_p+\mathbf{v}_a s$. Fourier analyzing the functions of s, we write

$$e^{i\mathbf{q}\cdot R_p}=\sum_{n=-\infty}^{\infty}a_n e^{in\omega_c s},$$
$$\mathbf{v}e^{i\mathbf{q}\cdot R_p}=\sum_{n=-\infty}^{\infty}\mathbf{v}_n e^{in\omega_c s}, \quad (17)$$

and obtain

$$j_e=\frac{e}{2\pi^2\hbar^2}\int_0^\infty dE\int_{-\infty}^\infty dk_z\left(-\frac{\partial f_0}{\partial E}\right)$$
$$\times\sum_{n=-\infty}^{\infty}\frac{m^*\mathbf{v}_n\cdot[e\mathcal{E}\cdot\mathbf{v}_n^*-(m/\tau)\mathbf{v}_n^*\cdot\mathbf{u}-(1/\tau)a_n^*\zeta_1]}{1/\tau+i(\omega-\mathbf{q}\cdot\mathbf{v}_a-n\omega_c)}. \quad (18)$$

It should be noted that ζ_1 is not a known parameter. If, however, we recall that collisions do not change the local electronic density, we obtain the condition

$$\int d^3k\tau^{-1}(f_1-f_2)=0. \quad (19)$$

If we now use Eq. (11) and proceed as above, we obtain

$$\int_0^\infty dE\int_{-\infty}^\infty dk_z\left(\frac{\partial f_0}{\partial E}\right)\sum_{n=-\infty}^{\infty}\frac{a_n[e\mathcal{E}\cdot\mathbf{v}_n^*-(m\mathbf{v}_n^*\cdot\mathbf{u}+a_n^*\zeta_1)(i\mathbf{q}\cdot\mathbf{v}_a+in\omega_c-i\omega)]}{1/\tau+i(\omega-\mathbf{q}\cdot\mathbf{v}_a-n\omega_c)}=0, \quad (20)$$

which completely determines ζ_1. It is now convenient to define the averages

$$\langle bc\rangle_1=\frac{m}{2\pi^2\hbar^2N}\int_0^\infty dE\int_{-\infty}^\infty dk_z\left(-\frac{\partial f_0}{\partial E}\right)$$
$$\times\sum_{n=-\infty}^{\infty}\frac{b_nc_n^*}{1+i(\omega-\mathbf{q}\cdot\mathbf{v}_a-n\omega_c)\tau}, \quad (21)$$

and

$$\langle bc\rangle_2=\frac{m}{2\pi^2\hbar^2N}\int_0^\infty dE\int_{-\infty}^\infty dk_z\left(-\frac{\partial f_0}{\partial E}\right)$$
$$\times\sum_{n=-\infty}^{\infty}\frac{b_nc_n^*i(n\omega_c+\mathbf{q}\cdot\mathbf{v}_a-\omega)\tau}{1+i(\omega-\mathbf{q}\cdot\mathbf{v}_a-n\omega_c)\tau}. \quad (22)$$

Also, at this point, we will assume for simplicity that τ is a constant; variations of τ over the Fermi surface are, in principle, easily included using the formalism given above. Solving Eq. (20), we obtain

$$\zeta_1=[\tau e\mathcal{E}\cdot\langle a\mathbf{v}\rangle_1-\langle a\mathbf{v}\rangle_2\cdot m\mathbf{u}]/\langle aa\rangle_2, \quad (23)$$

and find that the electronic current density is given by

$$j_e=\frac{Ne^2\tau}{m}\left\{\left[\langle m^*\mathbf{v}\mathbf{v}\rangle_1-\frac{\langle m^*\mathbf{v}\mathbf{a}_1\rangle\langle a\mathbf{v}\rangle_1}{\langle aa\rangle_2}\right]\cdot\mathcal{E}\right.$$
$$\left.-\left[\langle m^*\mathbf{v}\mathbf{v}\rangle_1-\frac{\langle m^*\mathbf{v}a\rangle_1\langle a\mathbf{v}\rangle_2}{\langle aa\rangle_2}\right]\cdot\frac{m\mathbf{u}}{e\tau}\right\}. \quad (24)$$

We may write this equation as

$$j_e=(\boldsymbol{\sigma}+\boldsymbol{\delta})\cdot\mathcal{E}-(\boldsymbol{\sigma}+\boldsymbol{\delta}')\cdot m\mathbf{u}/e\tau, \quad (25)$$

where the coefficients of $\mathcal{E}$ and $\mathbf{u}$ are given by

$$\boldsymbol{\sigma}=\sigma_0\langle m^*\mathbf{v}\mathbf{v}\rangle_1,$$
$$\boldsymbol{\delta}=-\sigma_0\langle m^*\mathbf{v}a\rangle_1\langle a\mathbf{v}\rangle_1/\langle aa\rangle_2, \quad (26)$$
$$\boldsymbol{\delta}'=-\sigma_0\langle m^*\mathbf{v}a\rangle_1\langle a\mathbf{v}\rangle_2/\langle aa\rangle_2,$$

and $\sigma_0=Ne^2\tau/m$ is the dc conductivity.

In order to compute the power absorbed Q it remains only to evaluate the expression in angular brackets in Eq. (7):

$$\left\langle\mathbf{p}\left(\frac{\partial f}{\partial t}\right)_{\text{coll}}\right\rangle_{\text{cy}}=\frac{2}{(2\pi)^3}\int d^3k\hbar K\frac{f_1-f_2}{\tau}. \quad (27)$$

Writing

$$\mathbf{k}e^{i\mathbf{q}\cdot R_p}=\sum_{n=-\infty}^{\infty}\mathbf{k}_n e^{in\omega_c s}, \quad (28)$$

we find

$$\left\langle\mathbf{p}\left(\frac{\partial f}{\partial t}\right)_{\text{coll}}\right\rangle_{\text{cy}}$$
$$=-\frac{m}{e\tau}\left\{(\boldsymbol{\sigma}_1+\boldsymbol{\delta}_1)\cdot\mathcal{E}-(\boldsymbol{\sigma}_1'+\boldsymbol{\delta}_1')\cdot\frac{m\mathbf{u}}{e\tau}\right\}, \quad (29)$$

where

$$\begin{aligned}\boldsymbol{\sigma}_1&=\sigma_0\frac{\hbar}{m}\langle m^*\mathbf{k}\mathbf{v}\rangle_1,\\ \boldsymbol{\delta}_1&=-\sigma_0\frac{\hbar}{m}\langle m^*\mathbf{k}a\rangle_2\langle a\mathbf{v}\rangle_1/\langle aa\rangle_2,\\ \boldsymbol{\sigma}_1'&=\sigma_0\frac{\hbar}{m}\langle m^*\mathbf{k}\mathbf{v}\rangle_2,\\ \boldsymbol{\delta}_1'&=-\sigma_0\frac{\hbar}{m}\langle m^*\mathbf{k}a\rangle_2\langle a\mathbf{v}\rangle_2/\langle aa\rangle_2.\end{aligned}\tag{30}$$

We now define

$$\begin{aligned}\boldsymbol{\Sigma}&=(\boldsymbol{\sigma}+\boldsymbol{\delta})/\sigma_0,\\ \boldsymbol{\Sigma}'&=(\boldsymbol{\sigma}+\boldsymbol{\delta}')/\sigma_0,\\ \boldsymbol{\Sigma}_1&=(\boldsymbol{\sigma}_1+\boldsymbol{\delta}_1)/\sigma_0,\\ \boldsymbol{\Sigma}_1'&=(\boldsymbol{\sigma}_1'+\boldsymbol{\delta}_1')/\sigma_0,\end{aligned}\tag{31}$$

and use Eqs. (25), (26), (27), (31), and (7) to show that

$$Q=-\tfrac{1}{2}\,\mathrm{Re}\,\mathrm{Ne}\mathbf{u}^*\cdot[(\mathbf{1}-\boldsymbol{\Sigma}_1)\cdot\boldsymbol{\mathcal{E}}-\boldsymbol{\Sigma}_1'\cdot m\mathbf{u}/e\tau].\tag{32}$$

Then using Eqs. (6) and (25) to determine the self-consistent field

$$\boldsymbol{\mathcal{E}}=-(\boldsymbol{\Gamma}/\sigma_0+\boldsymbol{\Sigma})^{-1}(\mathbf{1}-\boldsymbol{\Sigma}')\cdot m\mathbf{u}/e\tau,\tag{33}$$

we obtain the final result for the power absorption

$$Q=(Nm/2\tau)\,\mathrm{Re}\mathbf{u}^*\cdot[(\mathbf{1}-\boldsymbol{\Sigma}_1)(\boldsymbol{\Gamma}/\sigma_0+\boldsymbol{\Sigma})^{-1}\times(\mathbf{1}-\boldsymbol{\Sigma}')-\boldsymbol{\Sigma}_1']\cdot\mathbf{u}.\tag{34}$$

It should be noted that in the case of a spherical Fermi surface, $\boldsymbol{\Sigma}'=\boldsymbol{\Sigma}_1=\boldsymbol{\Sigma}$ and $\boldsymbol{\Sigma}_1'=\boldsymbol{\Sigma}-\mathbf{1}$, and it is easily seen that the results reduce to those of Cohen, Harrison, and Harrison.[10]

In this paper we use the general result of Eq. (34) to calculate the coefficient of ultrasonic attenuation in potassium for both SDW and free-electron models. The property of the SDW state of immediate interest is its nonspherical Fermi surface. For the linear SDW postulated for potassium, the Fermi surface resembles a lemon drawn out to a point in both directions along the dc magnetic field $\mathbf{B}$.

In both models cited above, the Fermi surface is axially symmetric about $\mathbf{B}$. For this symmetry, it may be seen that $\boldsymbol{\Sigma}$ and $\boldsymbol{\Sigma}'$ are identical; further, for the frequencies used in our experiments, 10^7–10^8 Hz, $\boldsymbol{\Gamma}/\sigma_0$ is much smaller than unity and can therefore be neglected. Equation (34) therefore reduces to

$$Q=\frac{Nm}{2\tau}\,\mathrm{Re}\mathbf{u}^*\cdot[\boldsymbol{\Sigma}^{-1}-\mathbf{1}+(\boldsymbol{\Sigma}_1-\boldsymbol{\Sigma}_1'-\boldsymbol{\Sigma}_1\boldsymbol{\Sigma}^{-1})]\cdot\mathbf{u}.\tag{35}$$

From the discussion following Eq. (34), it is obvious that the term $(\boldsymbol{\Sigma}_1-\boldsymbol{\Sigma}'-\boldsymbol{\Sigma}_1\boldsymbol{\Sigma}^{-1})$ vanishes for a spherical Fermi surface. Because the Fermi surface of the SDW state is nearly spherical, this term is small and can be neglected in any further discussion of this state. Finally, we see that the power absorption may be obtained, to a good approximation, in both models from the expression

$$Q=(Nm/2\tau)\,\mathrm{Re}\mathbf{u}^*\cdot[\boldsymbol{\Sigma}^{-1}-\mathbf{1}]\cdot\mathbf{u}.\tag{36}$$

In order to calculate $\boldsymbol{\Sigma}=(\boldsymbol{\sigma}+\boldsymbol{\delta})/\sigma_0$ from Eqs. (26) and (31), we require the coefficients $\mathbf{v}_n$ and a_n. It is readily shown that

$$\mathbf{v}_n=(-i)^n\begin{bmatrix} iv_\perp & J_n'(q_yv_\perp/\omega_c)\\ (n\omega_c/q_y) & J_n(q_yv_\perp/\omega_c)\\ v_z & J_n(q_yv_\perp/\omega_c)\end{bmatrix},\tag{37}$$

and

$$a_n=(-i)^nJ_n(q_yv_\perp/\omega_c).\tag{38}$$

We have assumed, without any loss of generality, that the wave vector of the sound wave lies in the y-z plane. In Eqs. (37) and (38) ω_c is the cyclotron frequency, v_z and $v_\perp$ are the electron velocities parallel and perpendicular to $\mathbf{B}$, and J_n and J_n' are the Bessel function of order n and its derivative, respectively. It can be seen from Eqs. (37), (38), (21), and (22) that, in order to compute the power absorption in both SDW and free-electron systems, it is only necessary to determine the parallel and perpendicular components of the electron velocity at the Fermi surface in each case. In the free-electron case this is straightforward; we give the calculation for a linear SDW in the next section.

III. ATTENUATION COEFFICIENT FOR SDW AND FREE-ELECTRON MODELS

As described by Overhauser,[5] the electronic wave function in the presence of a linear spin-density wave is a solution of the Schrödinger equation

$$(H_0+A)\psi=E\psi.\tag{39}$$

H_0 is the kinetic energy plus the diagonal part of the exchange energy, and A is the off-diagonal part. For a linear SDW of wave vector $\mathbf{Q}$ oriented in the z direction, A can be represented by the matrix,

$$A=-g\begin{bmatrix}0 & e^{-iQz} & 0\\ e^{iQz} & 0 & e^{-iQz}\\ 0 & e^{iQz} & 0\end{bmatrix}\tag{40}$$

connecting state $|\mathbf{k}\rangle$, spin up, with $|\mathbf{k}+\mathbf{Q}\rangle$, spin down, and with $|\mathbf{k}-\mathbf{Q}\rangle$, spin down. Treating A in first-order perturbation theory gives the secular equation

$$\begin{vmatrix}\epsilon_{\mathbf{k}-Q}-E & -ge^{-iQz} & 0\\ -ge^{iQz} & \epsilon_{\mathbf{k}}-E & -ge^{-iQz}\\ 0 & -ge^{iQz} & \epsilon_{\mathbf{k}+Q}-E\end{vmatrix}=0,\tag{41}$$

where ϵ_k is an eigenvalue of H_0. With the following definitions:

$$\begin{aligned}b&=-(\epsilon_{\mathbf{k}+Q}+\epsilon_{\mathbf{k}}+\epsilon_{\mathbf{k}-Q}),\\ c&=\epsilon_{\mathbf{k}-Q}\epsilon_{\mathbf{k}}+\epsilon_{\mathbf{k}+Q}\epsilon_{\mathbf{k}}+\epsilon_{\mathbf{k}-Q}\epsilon_{\mathbf{k}+Q}-2g^2,\\ d&=-\epsilon_{\mathbf{k}-Q}\epsilon_{\mathbf{k}+Q}\epsilon_{\mathbf{k}}+g^2(\epsilon_{\mathbf{k}+Q}+\epsilon_{\mathbf{k}-Q}),\\ p&=\tfrac{1}{3}b^2-c,\\ r&=2b^3/27-\tfrac{1}{3}bc+d,\end{aligned}\tag{42}$$

the three roots of Eq. (41) can be expressed as

$$E=-\tfrac{1}{3}b+\tfrac{2}{3}p^{1/2}\cos(\tfrac{1}{3}\phi+\tfrac{2}{3}\pi n), \quad (43)$$

where n may take the values 0, 1, or 2, and

$$\phi=\tan^{-1}[\pm(4p^3/27r^2-1)^{1/2}]. \quad (44)$$

Care must be taken to choose the value of n and the correct sign in Eq. (44) to ensure that Eq. (43) describes the lowest branch of the dispersion relation. The velocities v_z and $v_\perp$ may be found by taking the appropriate derivatives with respect to $\mathbf{k}$ of Eq. (43).

The model has three parameters which remain to be determined, $\mathbf{Q}$, g, and E_F(SDW), the Fermi energy in the SDW model. The parameter g can be seen to equal $\frac{1}{2}G$, where G is the gap between the upper and lower branches of the SDW spectrum at $k_z=\frac{1}{2}Q$. This parameter can be determined by supposing with Overhauser[5] that the peak in the optical absorption data of potassium found by Mayer and El Naby[4] may be attributed to an SDW state. In order to explain the shape of the peak, and also to account for the de Haas–van Alphen data on potassium, it is also necessary to assume that the Fermi surface touches the SDW "zone boundary" at only one point, namely $\frac{1}{2}Q$. This assumption leads to the condition $v_\perp=0$ at $k_z=\pm\frac{1}{2}Q$. Noting also that the volume enclosed by the Fermi surface must be equal to that of a free-electron sphere for the same density, we obtain the parameters Q and E_F(SDW). We find

$$\begin{aligned} g&=0.31\text{ eV},\\ Q&=1.063\times(2k_F),\\ E_F(\text{SDW})&=0.902E_F, \end{aligned} \quad (45)$$

where k_F and E_F refer to the free-electron model. This completely specifies the SDW spectrum and velocities.[14]

By using the perpendicular and parallel components of the electron velocities determined above, we can now compute the attenuation for propagation at arbitrary angles to the magnetic field for both models. Because the attenuation coefficient involves an infinite sum containing Bessel functions, as can be seen from Eqs. (21) and (37), a procedure was employed in the numerical calculations to retain a sufficient number of terms in the sum to insure accuracy. This procedure was simply to keep all terms involving Bessel functions of order n up to at least $(qv_\perp/\omega_c)+2$.

In Fig. 3, we plot the attenuation as a function of magnetic field at an angle of propagation of 50 deg and $ql=50$, and in Fig. 4, we give the derivative of this curve in the neighborhood of the edge. These curves exhibit several interesting features. As the magnetic field is reduced, the SDW curve exhibits a pronounced

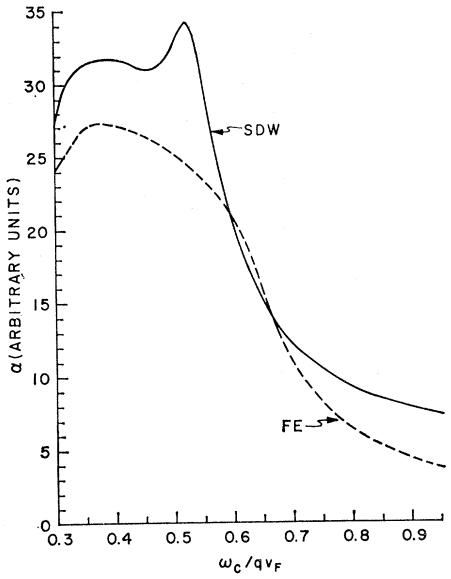

FIG. 3. A graph of the theoretically predicted attenuation, in arbitrary units, as a function of magnetic field, in the neighborhood of the absorption edge. The abscissa is given in units of ω_c/qv_F. Both free-electron and SDW curves are appropriate to an angle of propagation of 50 deg, and a ql value of 50.

maximum in the attenuation immediately following a sharp increase. By contrast, the free-electron curve behaves like a conventional Doppler-shifted cyclotron resonance edge. It should be noted that the theoretical edge, predicted by the inequality (1), falls close to the inflection point in the free-electron curve, whereas in the SDW model it coincides with the maximum. The maximum results from the existence of an integrable singularity in the number of states on the Fermi surface of velocity v_z satisfying the resonance condition. For

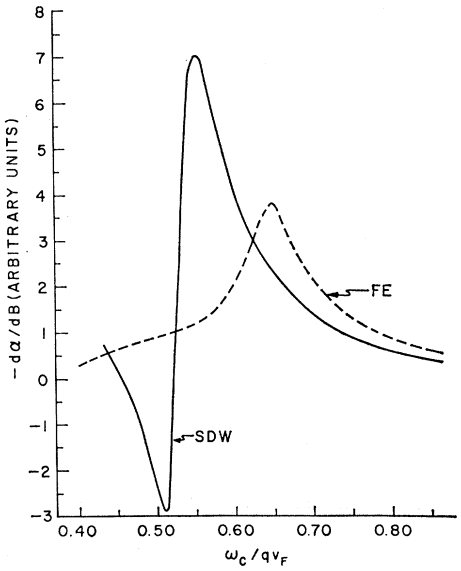

FIG. 4. A graph of the negative of the derivative of the attenuation given in Fig. 3 versus magnetic field.

[14] With these values of the SDW parameters the extremal cross section of the Fermi surface perpendicular to the magnetic field is 0.87% smaller than the free-electron value. This value is in essential agreement with that cited by Overhauser, Bull. Am. Phys. Soc. **10**, 39 (1965). We also remark, as shown in Fig. 2, that $v_M=0.82v_F$.

smaller values of ql, the peak will be smeared out and the two cases become difficult to distinguish. The differences are more striking, however, when we look at the derivative of the attenuation. (We actually plot $-\partial\alpha/\partial\beta$ in Fig. 4.) Here the peaks corresponding to the inflection points in Fig. 3 are seen to be separated by about 19%, as expected from the simple picture. It may also be noted that the shapes of the two curves are quite different, the SDW curve displaying a sharp minimum just below the edge. Again, we expect the differences between the two curves to be less pronounced at lower values of ql. In particular, the minimum in the SDW curve will disappear when $1/ql$ becomes large compared to the width of the peak in the density of states.

IV. EXPERIMENTAL PROCEDURE

Single-crystal potassium, in the form of cylindrical slices 0.5 in. thick and 1 in. in diameter, was obtained from Professor P. Meijer. The major axis of these slices was along the [110] direction. Cylinders $\frac{3}{8}$ in. in diameter (axis still along [110]), were spark cut from these slices and mounted, using conductive epoxy, in brass rings whose i.d. was the same as that of the spark cutting tool. The brass-ring technique was employed because it allowed the very soft potassium to be easily handled. It also offered the advantage that the brass spark cuts much more slowly than the potassium. This was important because flat and parallel acoustic surfaces were obtained by spark-planing the ends of the brass-ring–potassium assembly. If potassium alone were being spark-cut, it would cut quickly and flow, producing poor acoustic surfaces. However, with the cutting rate set by the much slower cutting brass ring, quite acceptable potassium surfaces were obtained. The one obvious danger of the above technique is the possibility of straining the potassium at low temperatures due to differential contraction of the brass-ring assembly. It was hoped that this effect would be minimal because the potassium shrinks more than the brass, and any straining must be due to the thin epoxy layer.

Bonds were made using Dow Corning 510 fluid of 60 000 centistoke viscosity.[15] The fluid was applied to potassium surfaces precooled to liquid nitrogen temperature to harden the potassium prior to the actual bonding operation. Ultrasonic echo patterns were checked at 77°K, and then the spring-loaded sample holder was rapidly immersed in the liquid-helium bath. Slow immersion was found to give consistently poor bonds at 4.2°K. Coaxially plated, 20 Mc/sec, X-cut quartz transducers were used to generate longitudinal waves in the samples.

A standard pulse-echo experimental arrangement was used to measure ultrasonic attenuation and velocity. Attenuation data, directly in decibel units, was presented on an x-y recorder whose y axis was fed by the output of a Matec Model 1235 Automatic Attenuation Recorder. The x axis was fed by the output of a Rawson-Lush Type 720 rotating-coil gaussmeter calibrated by NMR. Magnetic field values determined with this probe are estimated to be accurate to one percent. Acoustic frequencies are estimated to be known to the same degree of accuracy. The longitudinal sound velocity for the sample studied, at 4.2°K, was measured to be 2.71×10^5 cm/sec with an accuracy of $\pm1.5\%$. This agrees quite well with the published value of Marquardt and Trivisonno.[16] Magnetic fields were provided by a 12-in. Harvey-Wells electromagnet capable of a maximum field near 15 kG.

Data were obtained for three potassium samples at acoustic frequencies up to 140 Mc/sec. The most extensive set of data was obtained for the third sample, and this set was analyzed for comparison with theory. Curves were obtained for variation of attenuation with magnetic field at fixed angles θ between 0 and 90 deg, as well as for attenuation as a function of angle at several fixed values of field. Measurements were performed at both 4.2 and 1.1°K, and a temperature dependence of the attenuation was observed. This was consistent with measurements of the third sample's resistivity ratio by the eddy-current-decay method.[17] This ratio was measured to be 6050 at 4.2°K, and increased by approximately 25% when the temperature was further reduced to 1.1°K. Similar behavior was observed for the other two samples.

Orientation of $\mathbf{B}$ at known angles to $\mathbf{q}$ was made possible by accurate determination of the magnet position for $\theta=90$ deg. Other angles were then obtained by appropriate rotation of the magnet yoke. The $\theta=90$ deg configuration, for a free-electron Fermi surface, corresponds to a symmetry point in a plot of attenuation versus angle in the presence of a sufficiently high magnetic field. This fact was utilized as follows: The sample holder was inserted into the liquid helium cryostat so that the condition $\theta=90$ deg was roughly satisfied. Attenuation was then recorded as a function of angle to locate more accurately the symmetry point. This point was taken to be $\theta=90$ deg, and is believed to be accurate to within 1 degree.

V. COMPARISON OF EXPERIMENT AND THEORY

For quantitative comparison of theory with experiment, one must determine accurately the value of the parameter ql. The usual procedure for determining it utilizes the fact that at sufficiently high magnetic

[15] H. J. Foster, Ph.D. thesis, Catholic University of America, 1964 (unpublished); National Bureau of Standards Report 8550, 1964 (unpublished); see also H. J. Foster, P. Meijer, and V. Mielczarek, Phys. Rev. 134, A1849 (1965).

[16] W. R. Marquardt and J. Trivisonno, J. Phys. Chem. Solids 26, 273 (1965).

[17] C. P. Bean, R. W. De Blois, and L. B. Nesbitt, J. Appl. Phys. 30, 1976 (1959).

fields the attenuation saturates. For longitudinal waves at 90 deg, the saturation value is a function of ql. A theoretical plot of $\Delta\alpha \equiv [\alpha(B=\infty)-\alpha(B=0)]_{\theta=90°}$ versus ql for a spherical Fermi surface is shown in Fig. 5. This curve crosses $\Delta\alpha=0$ at $ql=6.81$. By experimentally measuring $\Delta\alpha$ for a given sample at several ultrasonic frequencies, and therefore at several different ql values, we may determine ql for any frequency by comparing with Fig. 5.

Curves of the form of Fig. 5 were found for both free-electron and SDW models by generalizing the procedure described above, viz., by defining

$$\Delta\alpha=\alpha(x_1)-\alpha(x_2), \tag{46}$$

where $x=\omega_c/qv_F$, and using the numerical calculations to determine the right-hand side. To avoid inaccuracies associated with the fact that the measured α versus B plots may not be fully saturated at the highest fields attained in the experiments, x_1 was chosen to be 2.10 rather than infinity. The corresponding value of B for 60 Mc/sec is 14.3 kG. The choice of x_2 presented more of a problem. When x becomes very small, the arguments of the Bessel functions become large, and many terms must be kept in the sums indicated in Eqs. (31) and (37) to insure sufficient accuracy of the final results. For the free-electron model it is possible to choose $x_2=0$ by the virtue of the fact that $\alpha(0)$ at 90 deg equals $\alpha(x)$ at 0 deg for arbitrary x. For the SDW aligned parallel to the field, $x_2=0.0596$ was used for two reasons: it corresponded to a magnetic field below the value where geometric resonance oscillations were observed, and the required number of Bessel functions was not prohibitive. From the experimental results at 4.2°K and acoustic frequencies of 20 and 60 Mc/sec, we obtained,

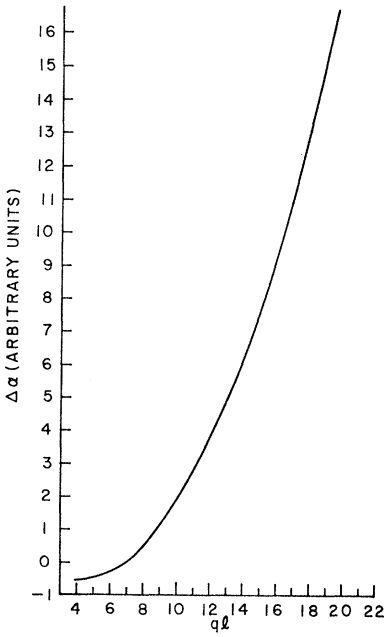

FIG. 5. A theoretical plot of $\Delta\alpha=[\alpha(B=\infty)-\alpha(B=0)]$, in arbitrary units, as a function of ql. This curve is appropriate to longitudinal waves propagating perpendicular to the dc magnetic field.

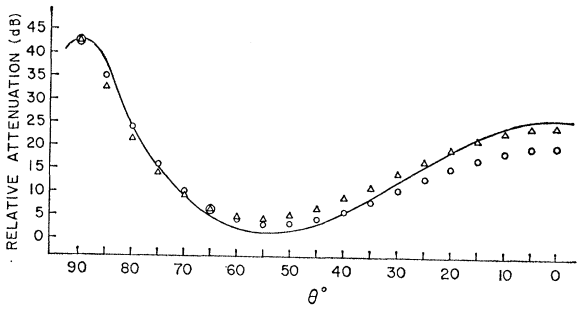

FIG. 6. A graph of relative attenuation, in decibel units, versus angle for a fixed magnetic field of 14.3 kG (corresponding to $\omega_c/qv_F=2.04$). The solid curve is the experimental result at a temperature of 4.2°K. The circles and triangles are the theoretical predictions of the SDW and free-electron models, respectively, fit at $\theta=90$ deg. The ql values used in the numerical calculations were determined with the aid of Fig. 5 to be 12.9 and 14.3 for the SDW and free-electron models, respectively.

for the higher frequency, ql values of 14.3 and 12.9 for the free-electron and SDW models, respectively.

In Fig. 6, we exhibit the experimental results for the attenuation as a function of angle at $x=2.04$. In addition, we show theoretical points for the free-electron and SDW models, with the ql values given above, fit to the experimental curve at 90 deg. The free-electron results should fit exactly at 0 and 90 deg; the observed small discrepancy represents an inconsistency between the completely isotropic free-electron model used here, and the experimental results.[18] The SDW is not expected to fit exactly at 0 deg since, for this case, zero field and zero angle are not equivalent. The inconsistency mentioned above, together with the relatively poor fit at intermediate angles, suggests that a more meaningful procedure would be to determine ql independently for each angle when comparing theoretical and experimental values of the attenuation as a function of field for fixed angle.

At a given angle, the right hand side of Eq. (46) may be calculated using the same values of x_1 and x_2 given above. When plotted against ql in the range $3\leq ql\leq 16$, the curve appears remarkably close to a straight line for angles of 40, 50, and 60 deg. The ql values obtained by comparing experimental $\Delta\alpha$ values with these curves are presented in Table I. The errors associated with reading $\Delta\alpha$ values from the experimental curves, and with the uncertainty in the acoustic frequencies, intro-

[18] A review of the experimental procedure revealed that, for very large attenuation (i.e., very small echo height), the detector section of the rf receiver has a square law instead of a linear response to incoming pulses. Consequently, the signal fed to the automatic attenuation recorder, for rectification and comparison with a fixed dc level, is smaller than would be the case with a linear response, and the recorded attenuation is too large. The potassium sample exhibits the highest attenuation at an angle of 90 deg for magnetic fields in the saturation region. In fact, in our measurements this attenuation was so large that the ultrasonic echoes dissappeared into the noise level of the receiver. This suggests that the measured saturation value of the attenuation at 90 deg may be erroneously high, and this small discrepancy may be entirely experimental.

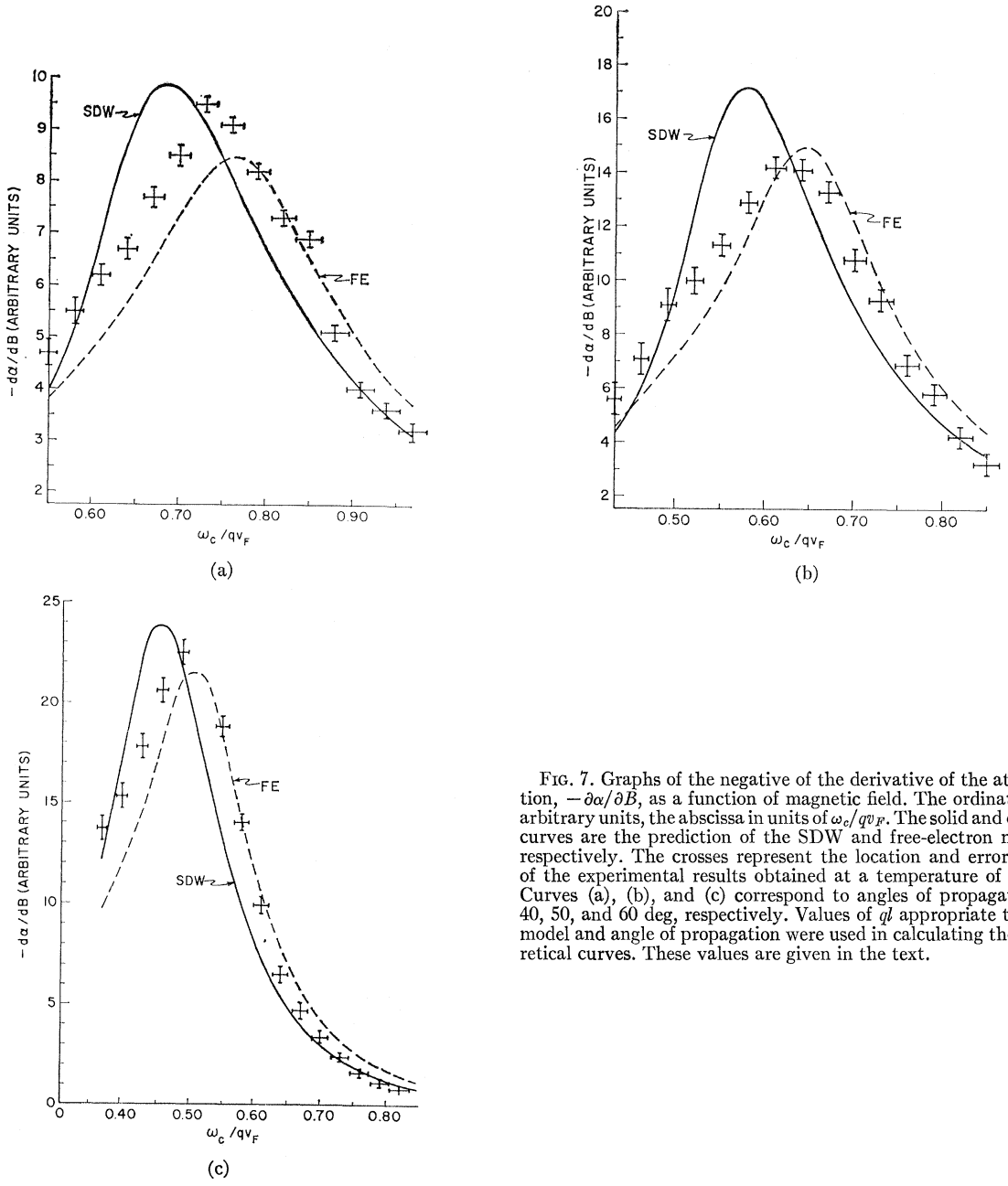

FIG. 7. Graphs of the negative of the derivative of the attenuation, $-\partial\alpha/\partial B$, as a function of magnetic field. The ordinate is in arbitrary units, the abscissa in units of ω_c/qv_F. The solid and dashed curves are the prediction of the SDW and free-electron models, respectively. The crosses represent the location and error limits of the experimental results obtained at a temperature of 1.1°K. Curves (a), (b), and (c) correspond to angles of propagation of 40, 50, and 60 deg, respectively. Values of ql appropriate to each model and angle of propagation were used in calculating the theoretical curves. These values are given in the text.

duce an inaccuracy of about 1% at 90 deg, while the determinations of ql at the other angles should be good to only about 10%. In both cases, the major source of error is the uncertainty in the frequencies, and the magnitude of the possible error is strongly dependent upon the functional relationship between $\Delta\alpha$ and ql.

TABLE I. Experimentally determined values of ql.

θ (deg)	FE	SDW
90	14.3	12.9
60	12.4	9.8
50	12.4	9.2
40	9.8	7.8

In Fig. 7 we display $-\partial\alpha/\partial B$ vs B at angles of 40, 50, and 60 deg. It is clear from Fig. 1 that at these angles, the edge is separated in field from other structure. Although these curves do not unambiguously distinguish between the two models, they do appear to favor the free-electron model.[19] It should be noted that the

[19] Recent measurements by Thomas and Bohm [R. L. Thomas and H. V. Bohm, Phys. Rev. Letters **16**, 587 (1966)] of the Kjeldaas absorption edge [T. Kjeldaas, Jr., Phys. Rev. **113**, 1473 (1959)] for shear waves propagating parallel to the dc magnetic field appear to favor the free-electron model.

40-deg curve, which does not appear to favor either model, corresponds to an unusually low value of ql.[20]

In addition to the absorption edge, there is other structure in the attenuation at lower fields. We now investigate this structure and compare it with the simple picture based on the free-electron model.[21] It is convenient to review first the familiar case of propagation at 90 deg. As we enter the regime $\omega_c/qv_F<1$, the conventional geometric resonances appear. These apparently arise when a matching condition between the orbital diameter of the belly ($k_z=0$) electrons and the sound wavelength $2\pi/q$ is satisfied. However, it is difficult to predict *a priori* what exactly the matching condition is in terms of the simple pictures of Fig. 8. With a naive interpretation, the situations depicted in Fig. 8(a) and 8(b) cannot be distinguished. If we assume that there are no collisions, we find in both cases that the component of the electric field in phase with the current must be zero (or, seen from another point of view, fields acting on an orbiting electron must induce currents of the same wavelength which are exactly out of phase). The other possibility convenient to our intuition is the local limit ($ql\ll1$). Then we find that in both cases (a) and (b), the field and current are in phase but the attenuations are equal. The actual situation lies somewhere between these two extremes and cannot easily be predicted without detailed knowledge of $\mathbf{\Sigma}(\mathbf{q},\omega)$.

We note from the calculation that as we reduce the field from high values, the first structure to appear in the attenuation is a minimum, and we may assume that this corresponds to the first matching condition to arise as orbit size is increased, that of Fig. 8(b). [The corresponding value of qv_F/ω_c from the calculation is 0.89π, instead of $\pi/2$, which might be more appropriate to Fig. 8(a).] As we lower the field, other maxima and minima appear, separated respectively by approximately $\Delta(qv_F/\omega_c)=\pi$, which tends to confirm the orbit matching hypothesis. The location of these extrema are given by the intercepts of the light lines in Fig. 1 with $\theta=90$ deg. These intercepts were taken directly from the numerical calculations appropriate to $ql=14.3$. The locations differ slightly from those given by Cohen, Harrison, and Harrison who assume $ql\gtrsim50$. The ql dependence of the positions of the extrema at 90 deg has recently been studied by Flax and Trivisonno.[22]

If we allow that situation (b) yields a minimum and

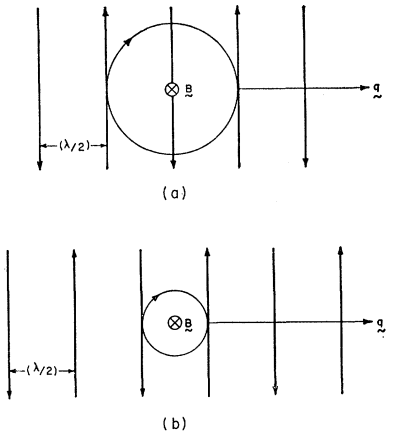

FIG. 8. A schematic representation of an acoustic wave propagating perpendicular to the dc magnetic field. The vertical arrows, separated by a half-wavelength of the sound wave, represent wave fronts at which the electric field is a maximum or minimum. The circles represent the orbits of an electron moving in the magnetic field. In case (a), the orbital diameter matches the acoustic wavelength; in case (b), it matches a half-wavelength.

(a) a maximum, then we may understand the increase and subsequent saturation of the attenuation at high fields, $\omega_c/qv_F\gtrsim2$. At large values of this parameter, the field is essentially constant over the entire orbit, a quintessential example of situation (a). Thus we may look at the high-field attenuation as corresponding to a broad maximum geometric resonance, which saturates when the orbit diameter is much smaller than the wavelength.

At oblique angles other types of geometric resonances, as well as the Doppler-shifted cyclotron resonance edges, appear. As an example, let us consider propagation at an angle θ to the dc magnetic field and, referring to Fig. 1, discuss the features observed in the attenuation as the field is lowered from high values. As we approach the value $\omega_c/qv_F=\cos\theta$, the attenuation increases due to the first Doppler-shifted cyclotron resonance edge, where the relation $\omega_c=q_zv_z$ is satisfied. Once we pass the point $\omega_c=q_zv_F$, this relation can always be satisfied for orbits at some value of $v_z<v_F$ and resonance absorption occurs. Thus, below the first cyclotron edge, we always have resonant contribution to the attenuation from the one particular orbit on the Fermi surface where $v_z=\omega_c/q_z$. This orbit is capable of satisfying a matching condition, when its projection in the direction of propagation matches the acoustic wavelength. This will give rise to geometric resonances in the Doppler-shifted cyclotron resonance absorption. It should be noted that these geometric resonances will, in general, be associated with nonextremal orbits. Once again, we have no way of knowing the precise nature of the matching condition, nor whether we will first see a maximum or minimum; both calculation and experiment show that in this case the first extremum is a maximum.

We can attempt to determine the positions of the

[20] The experimental points shown in Fig. 7 were obtained at a temperature of 1.1°K. Due to insufficient low-frequency data at that temperature, ql values used in the theoretical calculations were obtained by scaling the values of Table I, and are 13.8, 14.8, and 11.3 for the free-electron model, and 10.9, 11.0, and 9.0 for the SDW model at 60, 50, and 40 deg, respectively. We would expect that if ql values were determined independently at a sufficiently low temperature, where phonon scattering is negligible, the variation with angle would disappear.

[21] For the additional structure considered in this section, the predictions of both the free-electron and SDW models are essentially indistinguishable for the values of ql considered here.

[22] L. Flax and J. Trivisonno, Phys. Letters **22**, 569 (1966).

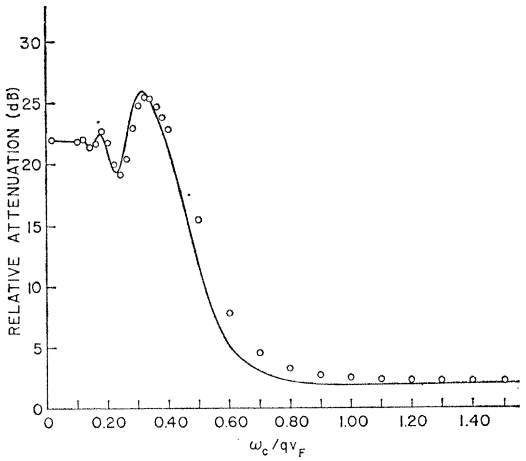

FIG. 9. A plot of the relative attenuation, in decibel units, as a function of magnetic field, measured in units of ω_c/qv_F. The solid curve is the experimental result obtained at a temperature of 4.2°K and an angle of propagation of 60 deg; the circles represent the prediction of the free-electron model for a ql value of 12.4.

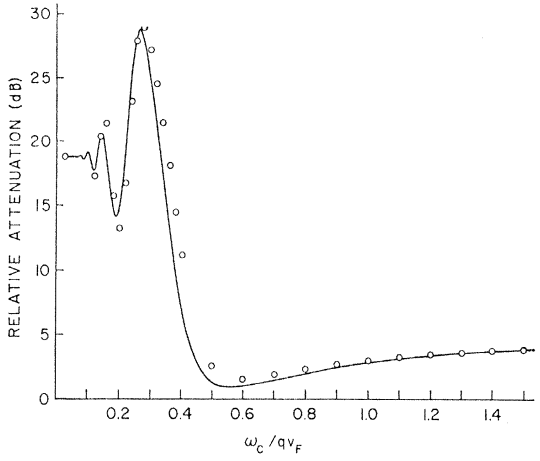

FIG. 10. A plot of relative attenuation versus magnetic field at an angle of propagation of 70 deg. The value of ql used in determining the theoretical points was 13.6. Other conditions are as given in Fig. 9.

extrema for oblique angles by a simple argument. The geometric resonances which appear at 90 deg can be extrapolated to oblique angles by assuming that the matching condition relates to the projection of the electronic orbit in the direction of propagation. This reasoning yields the light solid curves of Fig. 1, where the 90 deg intercepts are the extrema obtained from the numerical calculations. The location of the extrema of the geometric resonances in the cyclotron absorption may be obtained from a similar argument. For large values of $q_z l$, the dominant contribution to the cyclotron resonance absorption comes from the orbit with $v_z = n\omega_c/q_z$. Here the integer $n=1, 2, \cdots$ is the order of the cyclotron resonance. The diameter of the orbit is $2v_\perp/\omega_c$, where, in the free-electron model, $v_\perp = v_F[1-(n\omega_c/q_z v_F)^2]^{1/2}$. The matching condition will match the projection of the orbital diameter in the direction of propagation with the sound wavelength. Again we do not know, *a priori*, the exact nature of the matching condition, but we expect the orbital projections corresponding to successive maxima (and minima) to approach a separation of one wavelength. In constructing the dashed curves of Fig. 1, we have assumed that the extrema occur at the maxima and zeros of $J_n^2(qv_\perp \sin\theta/\omega_c)$. The heavy dashed curves show the first two extrema of J_1^2, and the light dashed curves those of J_2^2. For completeness, the first and second cyclotron edges are also included. The triangles and circles represent, respectively, the maxima and minima observed experimentally.

A detailed comparison of theory and experiment is shown in Fig. 9 and 10 for angles of propagation of 60 and 70 deg, respectively.[23] Here, the solid curve is the experimental result, and the open circles represent the theoretical calculations for the free-electron model at the value ql appropriate to the angle. Both curves are characterized by an abrupt rise in attenuation near the position of the first cyclotron edge. The first maxima can be assigned to the first extremum of J_1^2. An additional reason for this assignment is the fact that the first maximum moves toward higher fields as the angle is decreased. The second maximum occurs at a field such that it may be assigned to the first extremum of J_2^2. The first minimum of the 70-deg curve appears to fit rather well the second extremum of J_1^2, whereas the first minimum of the 60-deg curve cannot be unambiguously assigned. The proximity of the $n=2$ edge and the first maximum of J_0^2 might tend to move the J_1^2 minimum to higher fields. We must conclude that although Fig. 1 is helpful in understanding the experimental results, it cannot replace a detailed calculation.

VI. CONCLUSION

The arguments of Sec. III show that a study of the position of the Doppler-shifted cyclotron resonance edge for propagation of longitudinal waves at oblique angles should unambiguously distinguish between the SDW and free-electron models for potassium. However, our results, although suggestive of the free-electron model, are not definitive. The reason for this is twofold: First, the low values of ql attained in the experiments tend to blur the distinction, and secondly, the ql values, measured independently for each model, differed in a direction which tends to move the curves closer together than those shown in Figs. 3 and 4. In analyzing their data, Thomas and Bohm[19] neglect this second point. It should also be reemphasized that in the SDW

[23] It should be pointed out that theoretical calculations show the electronic attenuation at high fields and angles between 50 and 60 deg to virtually disappear. Thus longitudinal attenuation at these angles may be useful in determining the total electronic attenuation.

model used in these analyses, **Q** has been assumed to remain aligned parallel to the field even as the field is lowered to zero. This assumption is certainly open to question. We suggest that a more definitive test of the SDW hypothesis might be possible if this experiment were repeated with a ql value of the order of 50 and a derivative technique used.

Some of the general features of the attenuation at oblique angles are worth emphasizing. As has been pointed out by Eckstein,[1] at high ql, the position of the Doppler-shifted cyclotron resonance edge gives a measure of $(m^*v_z)_{\max}$, where m^* is the cyclotron effective mass. An additional point emphasized by Eckstein,[1] applicable to materials in which v_s/v_F is an order of magnitude larger than in simple metals like potassium, or in which ql is very large, is experimentally useful. This is the appearance of double edges. The observation of double edges facilitates the identification of the edge position, and allows both m^* and $(v_z)_{\max}$ to be determined independently. Finally, we note that although the geometric resonances associated with nonextremal orbits can, in principle, be used to map out the Fermi surface, in practice, it appears that this will be very difficult.

ACKNOWLEDGMENTS

The authors would like to thank Professor G. Seidel for many useful discussions and to acknowledge the helpful contributions of Professor R. Peverly.

PHYSICAL REVIEW VOLUME 156, NUMBER 3 15 APRIL 1967

Coherent-Potential Model of Substitutional Disordered Alloys

PAUL SOVEN
Bell Telephone Laboratories, Murray Hill, New Jersey
(Received 22 November 1966)

We introduce a model of a substitutional alloy based on the concept of an effective or coherent potential which, when placed on every site of the alloy lattice, will simulate the electronic properties of the actual alloy. The coherent potential is necessarily a complex, energy-dependent quantity. We evaluate the model for the simple case of a one-dimensional alloy of δ-function potentials. In order to provide a basis for comparison, as well as to see if a simpler scheme will suffice, we also calculate the spectrum of the same alloy using the average t-matrix approximation introduced by Beeby. On the basis of these results, we conclude that the average t-matrix approximation is not adequate for the description of an actual transition-metal alloy, while the coherent-potential picture will provide a more reasonable facsimile of the density of states in such an alloy.

I. INTRODUCTION

THE work reported here was stimulated by an attempt to find a reasonably simple and numerically tractable formalism for calculating the electronic structure of a metallic alloy. We desired a scheme whereby the density of states and the position of the energy bands could be determined.

At present very little is known concerning the electronic spectra of real alloys. There is, however, a great deal of information on the spectra of hypothetical one-dimensional alloys,[1–4] most of which is quite discouraging to someone attempting to find tractable formulas for the density of states. In the simple case of a one-dimensional alloy of δ-function potentials the density of states is extremely irregular,[4] possessing fine structure over energy intervals of the order of a few percent of typical bandwidths. This is to be compared with the structureless density of states function for an ordered lattice of δ functions. It is not likely that simple formulas can be devised to yield the alloy spectrum in detail. Our aim, therefore, was to find expressions which, when applied to the one-dimensional case, would effectively average the exact density of states over energy intervals sufficiently small so that gross distortions were not introduced into the spectrum. From this point of view, the better the formula, the smaller the energy interval over which it yields an average of the exact density of states. In accordance with this view, we will compare the approximate calculations of the cumulative, rather than the differential, density of states with the results of exact calculations.

The exact results to which we refer are necessarily for a one-dimensional crystal. The problem of calculating the spectrum of such an alloy has been extensively treated in the literature[2–5] and we will not dwell on it further except to say that the explicit numerical results for the cumulative density of states used for com-

[1] J. M. Luttinger, Phillips Res. Rept. **6**, 303 (1951).
[2] A. M. James and A. S. Ginzbarg, J. Phys. Chem. **57**, 840 (1953).
[3] R. Landauer and J. C. Helland, J. Chem. Phys. **22**, 1955 (1954).
[4] R. L. Agacy and R. E. Borland, Proc. Phys. Soc. (London) **84**, 1017 (1964).
[5] H. Schmidt, Phys. Rev. **105**, 425 (1957).